Science MS#1212896
The multielectron ionization dynamics underlying attosecond strong field spectroscopies

Andrey E. Boguslavskiy,[1] Jochen Mikosch,[1] Arjan Gijsbertsen,[1,2] Michael Spanner,[1]
Serguei Patchkovskii,[1] Niklas Gador,[3] Marc J.J. Vrakking,[2,4] and Albert Stolow[1]

[1]*Steacie Institute for Molecular Sciences, National Research Council of Canada, Ottawa, ON, Canada K1A 0R6*
[2]*FOM instituut voor atoom- en molecuulfysica (AMOLF), Science Park 102, 1098 XG Amsterdam, The Netherlands*
[3]*Department of Chemical Physics, Lund University, Box 124, SE-22100 Lund, Sweden*
[4]*Max-Born-Institute, Max Born Strasse 2A, D12489, Berlin, Germany*

(Dated: December 16, 2011)

Sub-cycle strong field ionization (SFI) underlies many emerging spectroscopic probes of atomic or molecular attosecond electronic dynamics. Extending methods such as attosecond high harmonic generation (HHG) spectroscopy to complex polyatomic molecules requires an understanding of multielectronic excitations, already hinted at by theoretical modelling of experiments on atoms, diatomics, and triatomics. Here we present a direct method which, independent of theory, experimentally probes the participation of multiple electronic continua in the SFI dynamics of polyatomic molecules. We show, using saturated (C_4H_{10}) and unsaturated (C_4H_6) linear hydrocarbons, how sub-cycle SFI of polyatomics can be directly resolved into its distinct electronic continuum channels by above threshold ionization photoelectron spectroscopy. Our approach makes use of photoelectron-photofragment coincidences, suiting broad classes of polyatomic molecules.

To date, measurements of attosecond electronic dynamics in atoms and molecules (1) have typically involved strong laser field processes. Even pump-probe spectroscopies using isolated attosecond pulses rely on the presence of a phased, strong ($\sim 10^{13}$ W/cm^2) laser field *(2–4)*. The process of high harmonic generation (HHG), which can probe electronic wave packets on attosecond time scales *(5–9)*, is entirely based on strong field ionization (SFI), as is the use of sub-cycle electron re-collision for probing dynamics *(10, 11)*. In the interpretation of experiments, broad use is made of the three-step model *(12)* wherein SFI adiabatically releases, via tunnelling, a single continuum electron which is subsequently driven in the strong, oscillating laser field. However, even in simple diatomics, the possible role of multiple electronic continua in attosecond SFI measurements *(5, 13, 14)* is unclear *(6, 15)*. In the complex world of multielectron polyatomic molecules, adiabatic, single electron tunnelling approximations are very unlikely to hold *(16–19)*. Nevertheless, to have broader impact, attosecond HHG spectroscopies must be extended to polyatomic molecules *(20)* and, therefore, a general understanding of the role of multielectron SFI dynamics in polyatomics is required. Here we introduce the Channel-Resolved Above Threshold Ionization (CRATI) method, where the channel refers to the electronic state of the ion correlated with the continuum electron. Independent of theoretical models, we experimentally resolve the multiple electronic continuum channels in SFI of polyatomic systems. By studying the CRATI of the linear hydrocarbons 1,3-butadiene and *n*-butane, we unambiguously demonstrate the direct, sub-cycle participation of multiple final ionic states in molecular SFI. We show that the population of higher-lying electronic continua can, depending on molecular properties, even exceed that of the ground state. We independently corroborate our experimental results with high level, all-electron dynamical Schrödinger equation calculations. These combined results show that the relative contributions of these multiple continuum channels depend on both molecular electronic structure and laser field properties, and that both adiabatic and non-adiabatic laser-driven electron dynamics may obtain.

A seminal attosecond transient absorption spectroscopy study recently demonstrated the coherent population (amplitudes and phases) of spin-orbit states following SFI of krypton atoms *(2)*. This technique benefited from the presence of sharp features in the absorption spectrum which identified the two coherently prepared ionic states. In order to discern the ionic states of polyatomic molecules populated by SFI, alternate approaches might be required, since transient absorption spectroscopy of polyatomics is much more complex. Our experimental approach is based on above threshold ionization (ATI) *(21–24)*, a universal SFI phenomenon wherein a field-driven continuum electron absorbs excess photons beyond the minimum number required for ionization. This leads to observation of a series of peaks in the electron kinetic energy spectrum, spaced by the photon energy. There is a deep relationship between ATI and the process of HHG. In both cases, sub-cycle SFI generates a continuum electron which, depending on phase, either recollides with its ion core and emits a burst of XUV radiation (HHG), or accelerates away from the ion as an energetic electron (ATI). In either case, a single cycle pulse would result in structureless HHG and ATI spectra. Structured spectra obtain from this sub-cycle emission (photon or electron) being repeated every optical cycle. First

evidence for the participation of multiple continua in HHG spectroscopy of molecules emerged from experiments on CO_2 *(5, 25)* N_2 *(6, 26, 27)* and N_2O_4 *(28)*, each relying strongly on theoretical modelling for interpretation. These results caution that essential multiple continuum effects should not be ignored. Such effects are to be expected in the SFI of polyatomic molecules because their many valence electrons should all respond to the strong laser electric field. We find, for the molecules studied here, that electrons can be ejected by tunnelling via independent channels, populating the ionic ground (ejection of the highest occupied molecular orbital electron—HOMO ionization) and/or excited (HOMO-1 etc. ionization) electronic states. By independent, we mean that these continuum channels remain uncoupled (i.e. no transitions between them) in the laser field. However, in other molecular systems and/or at higher laser intensity, non-adiabatic interchannel coupling can occur during SFI. In this situation, another bound electron makes a laser-induced transition on a sub-cycle timescale while the continuum electron is departing. This process is termed non-adiabatic multielectron (NME) ionization *(16)* and will be discussed below. Whether the response is adiabatic or not, population of multiple electronic continua will be a generic feature of SFI of polyatomic molecules. In order to distinguish SFI channels populating the ionic ground state continuum from those populating ionic excited state continua, we make use of the fact that, unlike diatomics, electronically excited polyatomic ions generally undergo rapid radiationless transitions leading to fragmentation *(29, 30)*. This is the case for the linear hydrocarbons studied here, 1,3-butadiene (C_4H_6) and *n*-butane (C_4H_{10}): only their ionic electronic ground state is stable, whereas transitions to electronically excited ionic states lead to unimolecular dissociation of the parent ion, producing fragments on a timescale much longer than the laser interaction *(31–33)*. However, in a strong laser field, fragment ions may also be produced by post-ionization excitation of the ionic ground state. Therefore, the observation of ionic fragmentation in itself does not constitute proof that the SFI process directly populates electronically excited ionic states. Experimentally, we need to distinguish two SFI pathways: (i) sub-cycle ionization directly into an ionic excited state vs. (ii) ionization forming the ionic ground state, followed by subsequent excitation during the laser cycles following ionization. In our CRATI experiment this is achieved by measuring the ATI kinetic energy spectrum in coincidence (or covariance) with parent and fragment ions. As described in the Supporting Online Material (SOM), the covariance mapping method reveals correlations between ions and electrons via statistical analysis of count rate fluctuations *(34)*. The ATI spectrum consists of a comb of electron kinetic energies spaced by the photon energy (eq.1):

$$E = m\hbar\omega - (I_p^{(D_j)} + U_p) \tag{1}$$

where m is an integer and $\hbar\omega$ is the photon energy. For the molecular core, the $I_p^{(D_j)}$ is the Stark-shifted molecular ionization potential of the j^{th} ionization channel (where $j = 0$ signifies the D_0 ground electronic state of the ion, $j = 1$ the D_1 first excited electronic state of the ion etc.), and accounts for the relative Stark shifts of both neutral and ionic states. Up is the ponderomotive (quiver) energy of a free electron (charge e, mass m_e) in an oscillating laser field of angular frequency ω and electric field amplitude E_0 (eq.2):

$$U_p = \frac{e^2 E_0^2}{4 m_e \omega^2} \tag{2}$$

As described in more detail in the SOM, the Stark-shifted ionization potential $I_p^{(D_j)}$ is the field-free ionization potential plus the difference in Stark shift between the neutral ground state and the j^{th} ionization channel. Due to their differing $I_p^{(D_j)}$, the different ionization channels will have ATI combs shifted with respect to each other. If direct SFI to an electronically excited ion state D_j occurs, the correlated ion fragments will exhibit an ATI comb shifted relative to that correlated with the parent ion. By contrast, if ion excited states were populated subsequently by post-ionization excitation, meaning that the continuum electron has departed before further excitation occurs, then the fragments would have the same ATI spectrum as the parent ion because post-ionization excitation can no longer influence the departed continuum electron. Note that while several electronically excited ionization channels might correlate with the same ion fragment, the parent ion will uniquely identify the D_0 ground state ionization channel. By our method, we can determine whether SFI directly produced ionic ground or excited states, or whether ionic excited states were sequentially populated following removal of the electron. In Tables 1 and S1 we list the vertical and Stark-shifted ionization potentials $I_p^{(D_j)}$ of the lowest four ionic electronic states for the molecules studied here. As seen from eqs. 1 and 2, the ATI shift depends on laser intensity and therefore spatial averaging over the laser focal volume reduces the contrast of the ATI peaks. As discussed in the SOM, we explicitly minimized this effect by using a restricted target volume geometry. We obtained absolute intensity calibrations by studying the shift of the ATI combs with laser intensity (i.e. U_p) for the H_2O molecule, in which the molecular Stark shifts are negligible. Coincidence experiments require that the ionization probability not be saturated, in which case ionization is spatially restricted to the very center of the laser focus so that the value of U_p in eq. 1 is very similar for all participating ionic states in the experiment. In SFI, possible excited state resonances in the neutral molecule can produce the well-known Freeman resonances *(35)*, leading to sharp features in the ATI spectra which have a limited progression. We indeed

observed Freeman resonances in these molecular systems (see Fig.S2 and accompanying text), as confirmed by their laser intensity independence. The ATI peaks, by contrast, shift monotonically with laser intensity. In low frequency fields the Freeman resonances contribute only to the first two or three ATI peaks: the shifts reported here are based on the higher members of the ATI progression. Therefore, the possible excitation of neutral excited states does not affect our analysis of the ATI shifts. By studying CRATI as a function of the ellipticity of the driving field, we furthermore confirmed that electron recollision played no significant role in producing excited states.

The details of the experimental geometry, data collection and analysis are presented in the SOM. In Fig. 1 we present the mass spectrum (left) and normalized CRATI photoelectron spectra (right) for 1,3-butadiene at a peak intensity of 1.9×10^{13} W/cm^2 ($\hbar\omega$=798 nm/1.55 eV, U_p=1.16 eV). The mass spectrum is strongly dominated by the parent ion $C_4H_6^+$, which accounts for 87% of the overall ion yield. This number directly gives a lower limit for the probability of formation of the D_0 ion electronic ground state in SFI of 1,3-butadiene, corresponding to HOMO ionization. A small (13%) contribution from fragments is also seen in the mass spectrum, indicating population of ionic excited states As a percent ratio of the parent ion signal, the most prominent fragmentation channels are $C_4H_5^+$ (1%), $C_3H_3^+$ (3%), and $C_2H_3^+$ (3%). The CRATI photoelectron spectra (right) show a series of peaks spaced by the photon energy, as expected. The CRATI peaks correlated with the parent $C_4H_6^+$ ion yield a comb associated with ionization into the X(D_0) ground state. In Fig.1 the vertical lines indicates the relative shifts of the ATI combs, determined from analysis of all peaks contributing to each comb. Relative to the $C_4H_6^+$ comb, the CRATI combs of the $C_4H_5^+$ and $C_3H_3^+$ fragment channels are both shifted towards lower energy by 0.95±0.05 eV, as determined by statistical analysis of the relative comb shifts. This is unambiguous experimental evidence of direct SFI into ion excited states in 1,3-butadiene: post-ionization fragmentation of the D_0 ground state could not produce this result. From Table 1, the Stark-shifted $D_1(^2A_u)$ and $D_2(^2A_g)$ states of the 1,3-butadiene ion lie 2.3 eV and 2.5 eV above the Stark-shifted $D_0(^2B_g)$ ground state, respectively. The ATI comb shift can only be observed modulo the photon energy (1.55 eV). Therefore, direct SFI to the $D_1(^2A_u)/D_2(^2A_g)$ states should produce an average CRATI comb shifted relative to that of the ground state by $2.40 - 1.55 = 0.85$ eV. Within errors, this is quantitatively the shift observed for the $C_4H_5^+$ and $C_3H_3^+$ CRATI combs. This conclusion is further supported by tuneable VUV single photon ionization studies on 1,3-butadiene, showing that the $C_3H_3^+$ and $C_4H_5^+$ fragments indeed appear as soon as the $D_1(^2A_u)$ ion state is energetically accessible *(32)*. By contrast, the $C_2H_3^+$ fragment has an appearance energy more than 6 eV above that of the parent ion *(32)*. In our experiment, $C_2H_3^+$ likely originates from further excitation of the ion in subsequent field cycles. As can be seen in Fig. 1, the $C_2H_3^+$ CRATI spectrum exhibits fairly washed out ATI structure with little modulation depth, consistent with several SFI channels contributing to the formation of this fragment. We can rule out the population of neutral excited states within the laser pulse, leading to their SFI and associated ATI comb: this is not consistent with the present results because the lower I_p (which determine their ATI comb shift) of a neutral excited state does not match those due to ionization of the neutral ground state.

In Fig. 2 we present mass (left) and CRATI spectra (right) for *n*-butane at a peak intensity of 1.6×10^{13} W/cm^2 ($\hbar\omega$=798 nm/1.55 eV, U_p=0.93 eV). In contrast to 1,3-butadiene, *n*-butane predominantly fragments upon ionization, producing $C_3H_n^+$ and $C_2H_n^+$ ions. The $C_3H_7^+$ and $C_3H_6^+$ fragments are associated with populating the first ionic excited state whereas the $C_2H_5^+$ fragment is known to be associated with the third ionic excited state *(33)*. Relative to the parent ion signal, the percent ratio of the fragment ions are: $C_3H_7^+$ (122%), $C_3H_6^+$ (27%), $C_2H_5^+$ (96%), and $C_2H_3^+$ (152%). Fig.2b shows that the $C_3H_7^+$ fragment CRATI comb (blue) is shifted to lower energy by 0.45 ± 0.05 eV relative to the parent ion comb (black). As seen in Table 1, the energy difference between the Stark-shifted D0 ion ground state and the field-split $D_1(^2B_g)$ / $D_2(^2A_g)$ ionic excited states of *n*-butane is 0.4 / 0.5 eV, in quantitative agreement with the shift of the $C_3H_7^+$ comb (blue) in Fig. 2. This reveals that the dominant $C_3H_7^+$ channel is due to direct SFI into the first excited ionic state. Fig. 2 also shows that the $C_3H_6^+$ CRATI comb (red) is shifted to lower energy by 0.40 ± 0.05 eV relative to the parent ion comb. Therefore, within experimental error, we can also associate $C_3H_6^+$ with direct SFI into the first ion excited state. The $C_2H_5^+$ (green) and $C_2H_3^+$ (see the SOM) fragment combs are both shifted to lower energy by 0.10 ± 0.05 eV relative to the parent ion comb. Although this shift is not in strict quantitative agreement with the data given in Table 1, within the approximations used in calculating the excited state polarizabilities, it is consistent with direct SFI into the third ion excited state. The CRATI results for *n*-butane show that SFI to electronically excited continuum channels can dominate over SFI to the ground state. In sum, the combined results of Figs. 1 and 2 experimentally demonstrate that multiple continua do participate in the direct SFI of polyatomic molecules, with the relative contributions of these channels depending upon molecular electronic structure. In the following, we interpret these observations in terms of the attosecond molecular SFI response.

The experimental results are independently (i.e. using no adjustable parameters) corroborated by all-electron, coupled-channel time-dependent Schrödinger equation (TDSE) calculations, outlined in detail in the SOM. Briefly, this mixed orbital/grid-based approach *(36)* makes no assumptions about the nature of the ionization mechanism or the adiabaticity of the field-driven electron response. The neutral ground state and the ground and excited ionic states are treated at an appropriate level of *ab initio* electronic structure theory. Both the bound electrons and the continuum electron are treated in the full three spatial dimensions whereas the nuclei are kept frozen at the ground state neutral

geometry. The only central approximations are that: (i) a finite number of final ion electronic states are included (7 for 1,3-butadiene, 8 for *n*-butane); and (ii) upon excitation, the departing electron is no longer anti-symmetrized with respect to the remaining ionic core electrons. Our method supports multiple electronic excitations within the neutral molecule. We calculated the channel-resolved ionization yields to each of the ionic electronic states. In order to compare with experiment, we additionally averaged these channel-resolved ionization rates over the random lab frame distribution of molecules axes. We calculated the ionization rates using a single half-cycle of the driving laser field, reflecting the sub-cycle ionization rates and excluding any multi-cycle response. The use of a half-cycle pulse is discussed and justified in the SOM. In Fig. 3a we present the results of the calculated channel-resolved SFI yields for the dominant conformers (inset) of 1,3-butadiene (left) and *n*-butane (right) at a peak intensity of 1.5×10^{13} W/cm^2. For 1,3-butadiene, ionization into the ionic ground state is the dominant channel, with some direct ionization into the first electronically excited state and higher lying channels. This result is in good agreement with the mass spectrum and CRATI results shown in Fig. 1. For the dominant anti conformer of *n*-butane (right) the calculations show that SFI into the first and higher lying electronically excited ionic states is favored over the ground state channel. Once again, this agrees well with the experimental mass spectrum and CRATI results for *n*-butane (Fig. 2). These theoretical results show that direct ionization into multiple ionic states can be understood as a sub-cycle phenomenon.

Qualitatively, the SFI response of these two molecules can be understood by considering the ionization energies and Dyson orbitals given in Table S4. The Dyson orbitals represent the initial single-particle state of the ionizing electron. Within the Hartree-Fock approximation and Koopmans picture, they become ionization channels from the HOMO, HOMO-1, HOMO-2, etc. In a tunnelling picture, SFI depends exponentially on the I_p through the Keldysh factor $\exp[-(2/3)(2I_p)^{3/2}/E_0]$. Furthermore, for diatomics *(37)* it is known that nodal planes in the Dyson orbitals can cause strong suppression of the total yield of SFI. For the case of 1,3-butadiene, although the 1^2A_u excited state has fewer nodal planes than the 1^2B_g ground state, the large energy gap favors the ground state. For the case of *n*-butane, where the energy gaps are much smaller, orbital symmetry effects become more pronounced. The Dyson orbitals for *n*-butane reveal that the 2^2A_g excited state has the fewest nodal planes and, hence, this state experiences the least suppression, rendering it the dominant SFI channel as seen in Fig.3a.

An important question is the role of laser-driven non-adiabatic interchannel coupling (also known as NME) in polyatomics. As discussed in the SOM, the hydrocarbons irradiated here at $\sim 10^{13}$ W/cm^2 peak intensity (798 nm) exhibited predominantly adiabatic multichannel SFI dynamics. However, at higher intensities, the role of NME in even simple diatomics remains under active debate *(6, 15)*. With our TDSE method, we can artificially turn off the laser-driven interchannel coupling in the theory and compare the result to the case where the coupling is retained. This procedure accentuates the effects of NME on the ionic state population distribution during SFI. We present in Fig. 3b theoretical channel-resolved SFI yields in *n*-butane using a higher intensity half-cycle pulse (1.5×10^{14} W/cm^2, 800 nm), both with (fuchsia) and without (turquoise) NME coupling. For simplicity, only the ^2A_g ground state and the ^2B_u excited state were included, as these are the continuum channels most strongly dipole coupled by the field. As seen in Fig. 3b, along two molecular frame directions x (middle) and y (right), coherent sub-cycle redistribution of population between electronic continuum channels occurs when NME is included. This qualitatively demonstrates that, at intensities typical of HHG experiments, the non-adiabatic population of multiple electronic continua can be another important contributor to the attosecond molecular response.

Although the present study does not address the tacit coherences created between ionic states *(2)*, the CRATI method directly reveals the population of multiple electronic continua in the SFI of polyatomic molecules. A future extension of this method which measures fragment ion energy and/or angular distributions will be of interest. Studying CRATI spectra as a function of molecular electronic structure, molecular frame alignment and laser frequency/intensity will illuminate the role of multiple electronic continua in attosecond SFI spectroscopies such as HHG.

[1] F. Krausz, M.Yu. Ivanov, *Reviews of Modern Physics* **81**, 163 (2009).
[2] E. Goulielmakis *et al.*, *Nature* **466**, 739, (2010).
[3] G. Sansone *et al.*, *Nature* **465**, 763, (2010).
[4] M. Uiberacker *et al.*, *Nature* **446**, 627 (2007).
[5] O. Smirnova *et al.*, *Nature* **460**, 972 (2009).
[6] S. Haessler *et al.*, *Nature Physics* **6**, 200 (2010).
[7] H.J. Wörner, J.B. Bertrand, D.V. Kartashov, P.B. Corkum, D.M. Villeneuve, *Nature* **466**, 604 (2010).
[8] J. Itatani *et al.*, *Nature* **432**, 867 (2004).
[9] C. Vozzi *et al.*, *Appl. Phys. Lett.* **97**, 241103 (2010).
[10] Y. Huismans *et al.*, *Science* **331**, 61, (2011).
[11] M. Meckel *et al.*, *Science* **320**, 1478, (2008).
[12] P.B. Corkum, *Phys. Rev. Lett.* **71**, 1994 (1993).

[13] X-B Zhou *et al.*, *Phys. Rev. Lett.* **102**, 073902 (2009).
[14] H. Akagi *et al.*, *Science* **325**, 1364 (2009).
[15] S. Petretti, Y.V. Vanne, A. Saenz, A. Castro, P. Decleva, *Phys. Rev. Lett.* **104**, 223001 (2010).
[16] M.Lezius *et al.*, *Phys. Rev. Lett.* **86**, 51 (2001).
[17] M. Smits, C.A. de Lange, A. Stolow, D.M. Rayner, *Phys. Rev. Lett.* **93**, 203402 (2004).
[18] A.N. Markevitch *et al.*, *Phys. Rev. A* **68**, 011402 (2003).
[19] Z.B. Walters, S. Tonzani, C.H. Greene, *J. Phys. Chem. A* **112**, 9439 (2008).
[20] D.J. Fraser *et al.*, *J. Phys. B* **28**, L739 (1995).
[21] P. Agostini, F. Fabre, G. Mainfray, G. Petite, N. Rahman, *Phys. Rev. Lett.* **42**, 1127 (1979).
[22] K.J. Schafer, B. Yang, L.F. DiMauro, K.C. Kulander, *Phys. Rev. Lett.* **70**, 1599 (1993).
[23] C.I. Blaga *et al.*, *Nature Physics* **5**, 335 (2009).
[24] H. Rottke, J. Ludwig, W. Sandner, *J. Phys. B: At. Mol. Opt. Phys.* **29**, 1479 (1996).
[25] X. Zhou *et al.*, *Phys. Rev. Lett.* **100**, 073902 (2008).
[26] B.K. McFarland, J.P. Farrell, P. H. Bucksbaum, M. Gühr, *Science* **322**, 1232 (2008).
[27] I. Thomann *et al.*, *J. Phys. Chem. A* **112**, 9382 (2008).
[28] W. Li *et al.*, *Science* **322**, 1207 (2008).
[29] P.B. Armentrout, T. Baer, *J. Phys. Chem.* **100**, 12866 (1996).
[30] W.A.Chupka, in *Chemical spectroscopy and photochemistry in the VUV*, eds. C. Sandorfy, P. Ausloos and M.B. Robin, NATO Advanced Study Institute Series (1974).
[31] R. Bombach, J. Dannacher, J.-P. Stadelmann, *J. Am. Chem. Soc.* **105**, 1824 (1983).
[32] J. Dannacher, J.-P. Flamme, J.-P. Stadelmann, J. Vogt, *Chem. Phys.* **51**, 189 (1980).
[33] W.A. Chupka, J. Berkowitz, *J. Chem. Phys.* **47**, 2921 (1967).
[34] L. J. Frasinski *et al.*, *Phys. Rev. A* **46**, R6789 (1992).
[35] R.R. Freeman *et al.*, *Phys. Rev. Lett.* **59**, 1092 (1987).
[36] M. Spanner, S. Patchkovskii, *Phys. Rev. A* **80**, 063411 (2009).
[37] J. Muth-Bohm, A. Becker, F.H.M. Faisal, *Phys. Rev. Lett.* **85**, 2280 (2000).
[38] G. Bieri, F. Burger, E. Heilbronner, J.P. Maier, *Chim. Acta* **60**, 2213, (1977).
[39] D.M.P. Holland *et al.*, *J. Phys. B: At. Mol. Opt. Phys.* **29**, 3091 (1996).
[40] L.J. Frasinski, K. Codling, P.A. Hatherly, *Science* **246**, 1029 (1989).
[41] D.M.P. Holland *et al.*, *J. Phys. B: At. Mol. Opt. Phys.* **29**, 3091 (1996).
[42] B.T. Pickup, *Chem. Phys.* **19**, 192 (1977).
[43] Y. Öhrn and G. Born, *Adv. Quantum Chem.* **133**, 1 (1981).
[44] M.W. Schmidt *et al.*, *J. Comput. Chem.* **14**, 1347 (1993).
[45] S. Patchkovskii, Z. Zhao, T. Brabec, and D.M. Villeneuve, *J. Chem. Phys.* **126**, 114306 (2007).
[46] D.E. Manolopoulos, *J. Chem. Phys.* **117**, 9552 (2002).
[47] AG, AEB and JM contributed equally to this work. We thank NSERC for financial support. J. Mikosch thanks the Feodor Lynen program of the Alexander von Humboldt Foundation for financial support. Aspects of this work are part of the research program of the "Stichting voor Fundamenteel Onderzoek der Materie (FOM)", which is financially supported by the "Nederlandse organisatie voor Wetenschappelijk Onderzoek (NWO)". The authors thank R. Lausten, B.J. Sussman, D.J. Moffatt and D. Guay for expert assistance. The authors declare no competing financial interests.

TABLE I: Vertical field-free ionization potentials I_P^{FF} and Stark-shifted ionization potentials I_P^{SS} (in eV) of the first four ionic states (D_j, $j = 0 - 3$) of *n*-butane and three ionic states (D_j, $j = 0, 1, 2$) of 1,3-butadiene. The I_P^{FF} are measured values were taken from *(38)* unless otherwise indicated. The I_P^{SS} include the calculated Stark shift of the j^{th} ionization potential, as described in the SOM. As the CRATI measurements were performed in presence of the laser field, the I_P^{SS} values pertain for comparison with experiment

		n-butane	1,3-butadiene
D_0	I_P^{FF}	11.2	9.29*
	I_P^{SS}	11.0	9.2
D_1	I_P^{FF}	11.7	11.48*
	I_P^{SS}	11.4	11.5
D_2	I_P^{FF}	11.7	12.2
	I_P^{SS}	11.5	11.7
D_3	I_P^{FF}	12.2	(not used)
	I_P^{SS}	12.2	

* Taken from *(39)*

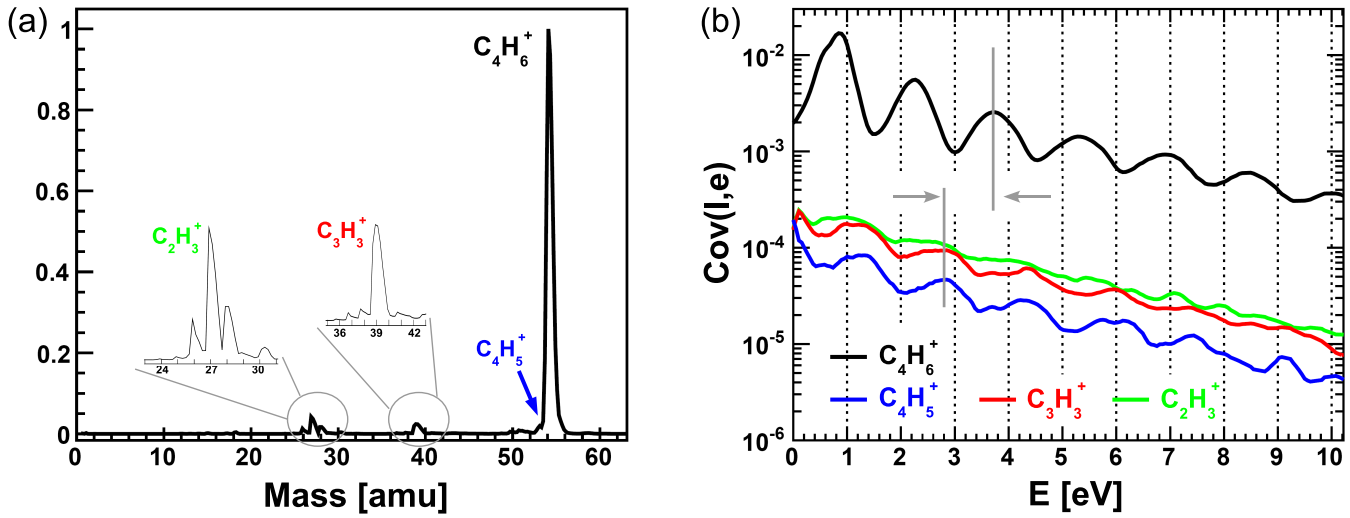

FIG. 1: Strong-field ionization of 1,3-butadiene at a peak intensity of 1.9×10^{13} W/cm^2. (a) Mass spectrum with the most prominent peak being the parent $C_4H_6^+$. Fragment ions $C_2H_3^+$, $C_3H_3^+$ and $C_4H_5^+$ that originate from the unstable D_1 excited ion state were also observed. (b) CRATI photoelectron spectra correlated with both parent and fragment ions. As indicated by the vertical lines, the fragment CRATI combs are shifted in energy relative to that of the parent ion (black) by 0.9 ± 0.05 eV. This is quantitatively the energy difference between the Stark-shifted D_0 and D_1 ionic states in 1,3-butadiene, modulo the photon energy, which unambiguously demonstrates that the excited D_1 ion state was directly populated from the neutral ground state. For a detailed discussion, see the text.

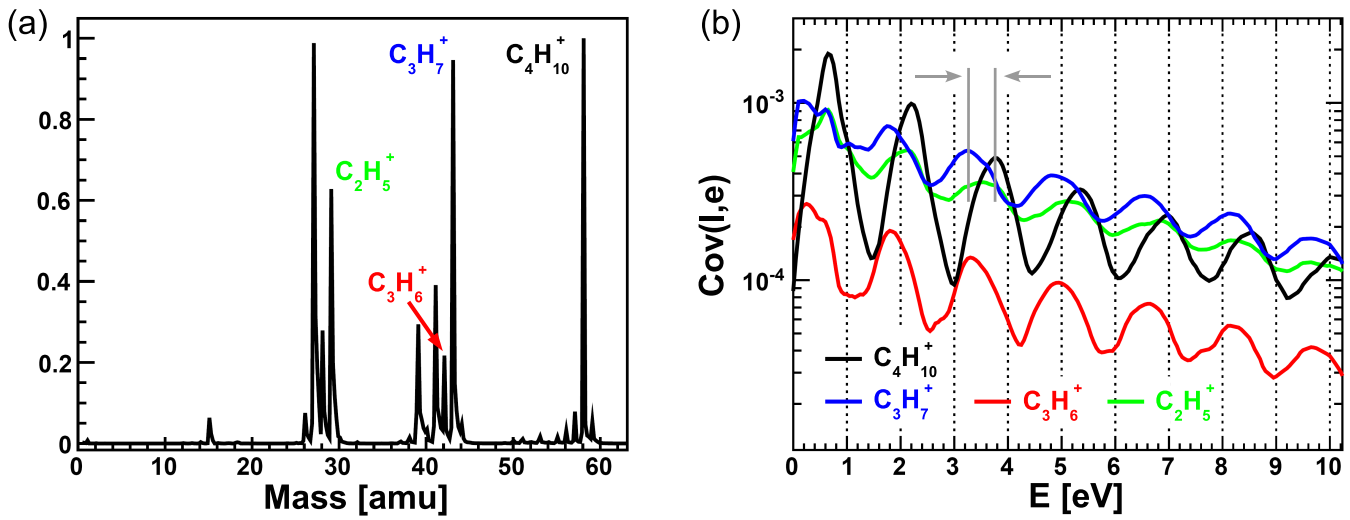

FIG. 2: Strong-field ionization of *n*-butane at a peak intensity of 1.6×10^{13} W/cm^2. (a) Mass spectrum. (b) CRATI photoelectron spectra correlated with different fragment ions. Extensive fragmentation occurs even at low intensity. Several fragment CRATI combs show a shift relative to that of the parent ion (black). These can be quantitatively assigned to originate from direct SFI into excited ionic states.

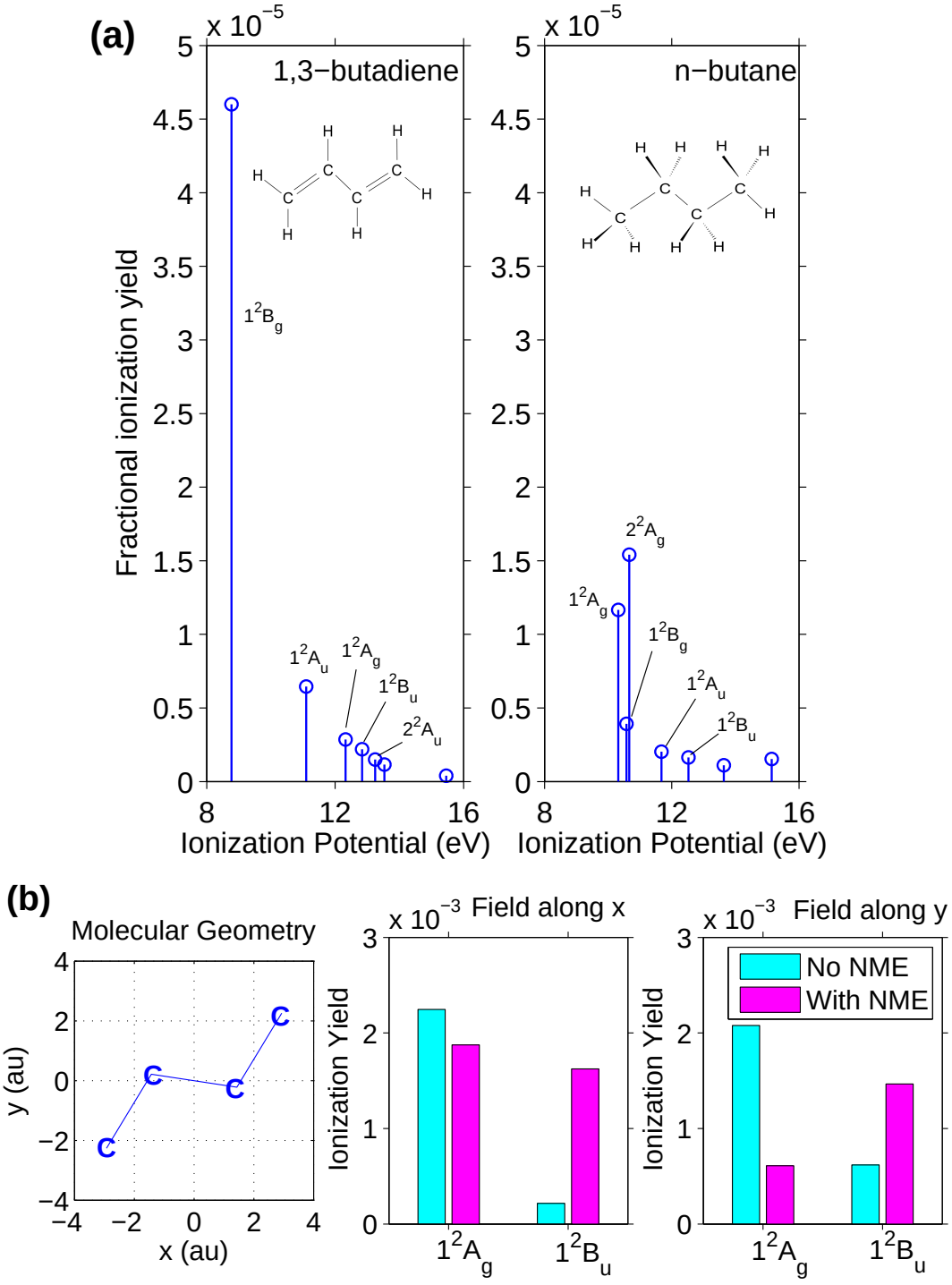

FIG. 3: (a) TDSE calculations of half-cycle ionization yields for producing the lowest few ionic states for the dominant conformers of 1,3-butadiene (left) and *n*-butane (right). The intensity was set to 1.5×10^{13} W/cm^2 at a wavelength of 800 nm. For 1,3-butadiene, ground state ionization is strongly favored, whereas for *n*-butane excited state ionization is more probable. For more details, see the SOM. (b) TDSE calculations of half-cycle ionization yields for *n*-butane into the ^2A_g ionic ground state and the strongest coupled ionic excited state (^2B_u), shown both with (fuchsia) and without (turquoise) laser-driven non-resonant inter-channel dipole coupling (also known as NME) between the ionic states, for a higher intensity of 1.5×10^{14} W/cm^2 at a wavelength of 800 nm. Channel resolved ionization yields for two molecular frame field directions, x and y, are presented in the middle and right hand panels, respectively. The left hand panel shows the *n*-butane molecular frame relative to the x and y axes. NME considerably impacts both ionization yields and electronic population redistribution amongst the ionic states within a half field cycle, and these effects are alignment sensitive. For more details, see the SOM.